than the L phase ($d^*_{25°C} \cong 210$ Å, $d^*_{60°C} \cong 170$ Å). If a match in d spacing is required for the L to $Q_{Ia\bar{3}d}$ transition, an even larger mismatch will further inhibit the L_c to $Q_{Ia\bar{3}d}$ transition. We have not observed a direct transition from L_c to $Q_{Ia\bar{3}d}$ in any PEO-PEE sample. Formation of the L phase upon heating from the L_c phase occurs because the phases are topologically identical, and therefore it appears that a large spacing mismatch does not inhibit this transition.

These low-MW PEO-PEE block copolymers appear to behave as both block copolymers and lyotropic LCs, and in fact most of the phase behavior reported here has been seen in both classes of amphiphiles (*2*, *13*, *14*, *26*–*29*). However, the length scale mismatch between the L and the $Q_{Ia\bar{3}d}$ phases is significantly enhanced in these polymers, and this mismatch inhibits the forward transition. These polymers highlight two important factors in soft material phase transitions: epitaxy and molecular conformation. We believe the large lattice mismatches in these polymers can be thought of as a consequence of "double frustration." Packing frustration in lyotropic systems occurs on only one side of the microdomain space because of the solvated state of the hydrophilic side (that is, water plus polar head group). The additional degree of freedom imparted by the water permits the system to accommodate a larger number of morphologies at fixed lattice spacing purely on the basis of the ability of the water to move relatively freely within the microdomain space. This freedom also appears to facilitate phase transitions. In a block copolymer melt, a single-component system, molecular conformation is "frustrated" on both sides of the microdomain space. However, increasing MW increases the number of conformational states available to the chains, and this appears to mitigate packing frustration (*14*, *26*). The large number of conformational states in high-MW block copolymers seems to play the same role that water does in the lyotropic systems. Therefore, differences in domain spacing between phases are either small or nonexistent.

The PEO-PEE block copolymers described here were designed to amplify the effects of double frustration. We have enhanced the frustration on both sides of the microdomain space by removing the water normally present in solvated nonionic surfactants and by decreasing the MW found in typical block copolymers. Those changes exaggerated the effects on ordered-state phase transitions. The addition of water or homopolymer to these block copolymers will enable us to test this hypothesis and move continuously from thermotropic block copolymer phase behavior to lyotropic block copolymer phase behavior in one system.

REFERENCES AND NOTES

1. R. G. Laughlin, *The Aqueous Phase Behavior of Surfactants* (Academic Press, San Diego, 1994).
2. J. M. Seddon, *Biochim. Biophys. Acta* **1031**, 1 (1990).
3. S. M. Gruner, *J. Phys. Chem.* **93**, 7562 (1989).
4. P. Mariani, V. Luzzati, H. Delacroix, *J. Mol. Biol.* **204**, 165 (1988).
5. Y.-S. Lee *et al.*, *J. Am. Chem. Soc.* **117**, 5573 (1995).
6. S. Puvvada, S. Baral, G. M. Chow, S. B. Qadri, B. R. Ratna, *ibid.* **116**, 2135 (1994).
7. A. Monnier *et al.*, *Science* **261**, 1299 (1993).
8. J. S. Beck *et al.*, *J. Am. Chem. Soc.* **114**, 10834 (1992).
9. J. Burgoyne, M. C. Holmes, G. J. T. Tiddy, *J. Phys. Chem.* **99**, 6054 (1995).
10. F. S. Bates, *Science* **251**, 898 (1991).
11. _____ and G. H. Fredrickson, *Annu. Rev. Phys. Chem.* **41**, 525 (1990).
12. S. Chandrasekhar, *Liquid Crystals* (University Press, Cambridge, 1992).
13. F. S. Bates, M. F. Schulz, A. K. Khandpur, S. Förster, J. H. Rosedale, *Faraday Discuss.* **98**, 7 (1994).
14. S. Förster *et al.*, *Macromolecules* **27**, 6922 (1994).
15. M. W. Matsen and F. S. Bates, *ibid.*, in press.
16. J. D. Mitchell, G. J. T. Tiddy, L. Waring, T. Bostock, M. P. McDonald, *J. Chem. Soc. Faraday Trans. 1* **79**, 975 (1983).
17. K. Kratzat and H. Finkelmann, *Colloid Polym. Sci.* **272**, 400 (1994).
18. M. A. Hillmyer and F. S. Bates, in preparation.
19. The PEE block in these block copolymers is an amorphous material with a glass transition temperature of approximately −30°C.
20. I. W. Hamley *et al.*, *Macromolecules* **26**, 5959 (1993).
21. S. S. Funari, M. C. Holmes, G. J. T. Tiddy, *J. Phys. Chem.* **98**, 3015 (1994).
22. For a complete discussion of the methods used to determine the microstructures of ordered block copolymers, see (*13*, *14*, *28*–*30*).
23. F. S. Bates and G. H. Fredrickson, *Macromolecules* **27**, 1065 (1994).
24. M. W. Matsen and M. Schick, *ibid.*, p. 4014.
25. M. Clerc, A. M. Levelut, J. F. Sadoc, *J. Phys. II (France)* **1**, 1263 (1991).
26. D. A. Hajduk *et al.*, *Macromolecules* **27**, 490 (1994).
27. D. A. Hajduk *et al.*, *ibid.*, p. 4063.
28. M. F. Schulz, F. S. Bates, K. Almdal, K. Mortensen, *Phys. Rev. Lett.* **73**, 86 (1994).
29. A. K. Khandupur *et al.*, *Macromolecules* **28**, 8796 (1995).
30. J. H. Rosedale, F. S. Bates, K. Almdal, K. Mortensen, G. D. Wignall, *ibid.*, p. 1429.
31. SANS experiments were conducted at the Risø National Laboratory, Denmark, with neutrons of 5.6 Å wavelength. The SAXS experiments were conducted at the CCLRC radiation source at Daresbury, UK, with x-rays of 1.50 Å wavelength. The fundamental interplanar spacing d^* is equal to $2\pi/q^*$, where q^* is the principal scattering wave vector. Selective deuteration of the PEE block in the synthesis of **OE10** provided large neutron scattering contrast. The PEO-PEE materials have substantial x-ray contrast.
32. Y. Rançon and J. Charvolin, *J. Phys. Chem.* **92**, 2646 (1988).
33. K. A. Koppi, M. Tirrell, F. S. Bates, K. Almdal, K. Mortensen, *J. Rheol.* **38**, 999 (1994).
34. Long-time annealing experiments and temperature quenches from the DIS state lead us to believe that the equilibrium phase at low temperature in **OE10** is $Q_{Ia\bar{3}d}$. Cooperative chain stretching induced by PEO block crystallization apparently resets the system to a nonequilibrium state. Application of large amplitude shear can have the same effect. Shearing a sample that was cooled from the $Q_{Ia\bar{3}d}$ state results in a spacing that is similar to the L spacing obtained on heating from the L_c state (see Fig. 4).

35. Supported by Air Force Office of Scientific Research grant AF/F49620-93-0182 and by the Center for Interfacial Engineering, an NSF Engineering Research Center. EPSRC is acknowledged for providing x-ray beam time. F.S.B. and K.A. benefited from a NATO travel grant. We thank M. Matsen and D. Hajduk for helpful discussions during the preparation of this manuscript.

3 October 1995; accepted 8 December 1995

Chain Migration of Neuronal Precursors

Carlos Lois, Jose-Manuel García-Verdugo, Arturo Alvarez-Buylla*

In the brain of adult mice, cells that divide in the subventricular zone of the lateral ventricle migrate up to 5 millimeters to the olfactory bulb where they differentiate into neurons. These migrating cells were found to move as chains through a well-defined pathway, the rostral migratory stream. Electron microscopic analysis of serial sections showed that these chains contained only closely apposed, elongated neuroblasts connected by membrane specializations. A second cell type, which contained glial fibrillary acidic protein, ensheathed the chains of migrating neuroblasts. Thus, during chain migration, neural precursors moved associated with each other and were not guided by radial glial or axonal fibers.

Neurons of the central nervous system of vertebrates originate in the ventricular zone (VZ) and subventricular zone (SVZ) (*1*) and from there migrate to reach their final destinations where they differentiate. Two forms of neuronal migration have been described in the developing brain (*2*): radial migration in which young neurons climb on the shafts of radial glial cells (*3*–*5*), and tangential migration, in which cells move parallel to the surface of the ventricles and perpendicular to the radial glial fibers (*6*–*11*). Tangential migration has been inferred from the dispersal of clonally related cells (*8*), from the orientation of migrating precursors (*7*, *9*, *10*), and from time-lapse studies of migrating cells in brain slices in vitro (*11*).

C. Lois and A. Alvarez-Buylla, Rockefeller University, 1230 York Avenue, New York, NY 10021, USA.
J.-M. García-Verdugo, Facultad de Biológicas, Universitas Valencia, Burjassot, Valencia 46100, Spain.

*To whom correspondence should be addressed.

Neurogenesis continues in the brain of some adult vertebrates (*12*) in which both radial and tangential migration have been described. In adult birds (*4*) and reptiles (*13*), young neurons migrate away from the ventricular walls along fibers of radial cells oriented perpendicularly to the ventricular surface. In neonatal and adult rodents, cells from the SVZ of the lateral ventricle migrate rostrally and differentiate into neurons in the olfactory bulb (*6*, *9*, *10*). This migration is tangential and occurs along a well-defined pathway, the rostral migratory stream (RMS). There is no evidence that radial glial fibers, axons, or cell processes guide this migration (*14*). Therefore, we have studied the mechanisms of neuroblast migration in the RMS of adult mice.

In a previous study we showed that cells in the RMS that express polysialylated neural cell adhesion molecule (PSA–N-CAM) are organized into chains (*15*). Similar chains were observed when the dye DiI was injected in the SVZ in the wall of the lateral ventricles to label migrating neuronal precursors (Fig. 1) (*16*). Migrating neuroblasts remained organized as chains until they reached the core of the olfactory bulb, from where they migrated radially as individual cells to more peripheral layers.

Staining with antibodies to vimentin or RC2 (*17*), markers of radial glial cells, did not reveal any fibers spanning the RMS. In addition, small crystals of DiI in the SVZ or olfactory bulb of fixed brains from adult mice (*18*) did not label fibers in the RMS, although axons were brightly labeled by DiI in other regions of the brain such as in the lateral olfactory track and corpus callosum. Together these results suggest that chains of migrating neuroblasts in the RMS are not guided by radial glial or axonal processes.

Immunocytochemistry with antibodies to glial fibrillary acidic protein (GFAP) (*19*), a marker of astrocytes (*20*), and with antibodies to PSA–N-CAM (*15*, *21*) revealed that these two molecules are especially abundant in the RMS (Fig. 2, A and C). At higher magnification, a meshwork of GFAP-positive processes (Fig. 2B) is visible surrounding PSA–N-CAM–positive chains (Fig. 2D). The GFAP immunoreactive cells had diverse shapes, and their branched processes were oriented in multiple directions (Fig. 2B).

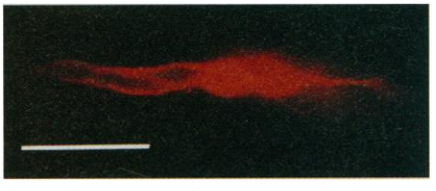

Fig. 1. Chain of migrating cells in the RMS 4 days after microinjection of DiI (*10*) into the SVZ in the wall of the lateral ventricle. Scale bar: 25 μm.

The immunocytochemical results suggested a relation between the migrating neuroblasts and GFAP-positive glial cells in the RMS. This relation was confirmed by electron microscopy (EM) (*22*). In sagittal sections, the migratory pathway appeared as

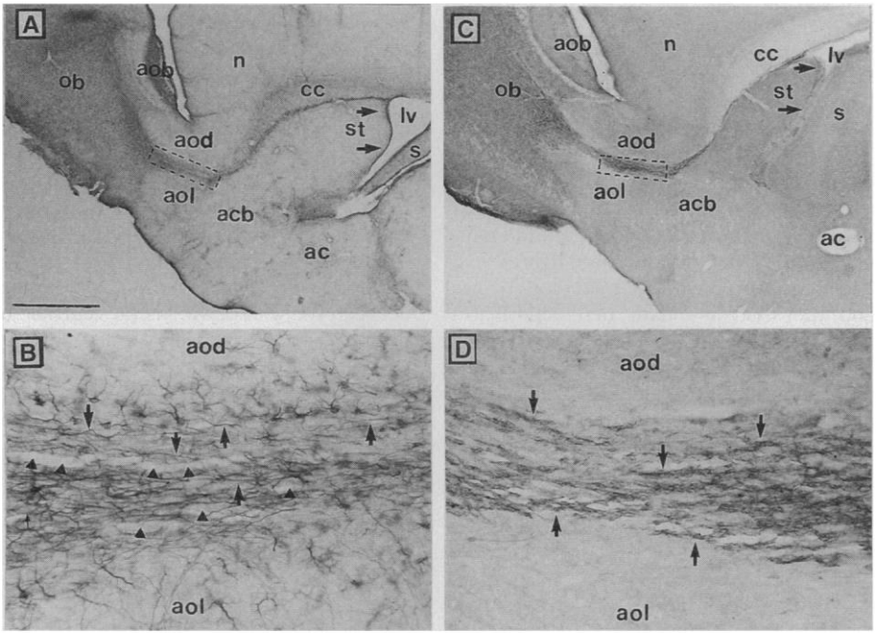

Fig. 2. (**A**) GFAP- and (**C**) PSA–N-CAM–immunoreactive cells are enriched in the RMS as shown in these sagittal sections of the anterior forebrain of adult mice. Dashed rectangles in (A) and (C) are the sectors of the RMS photographed at higher magnification in (B) and (D). (**B**) GFAP-positive processes (solid arrows) in the center of the RMS. Notice the elongated spaces (arrowheads) not stained by GFAP antibodies. (**D**) Chains of PSA–N-CAM–immunopositive cells (arrows) in the RMS. Arrows in (A) and (C) point at the SVZ of the lateral ventricle. lv, lateral ventricle; s, septum; st, striatum; ob, main olfactory bulb; acb, nucleus accumbens; cc, corpus callosum; n, neocortex; aob, accessory olfactory bulb; aol, lateral part of the anterior olfactory nucleus; aod, dorsal part of the anterior olfactory nucleus. Scale bar: (A) and (C), 1 mm; (B) and (D), 20 μm.

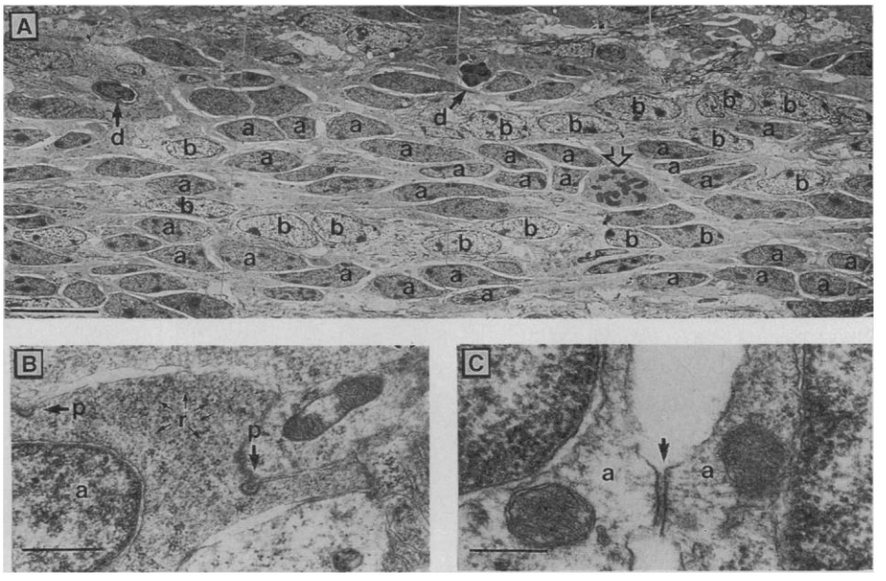

Fig. 3. Sagittal electron micrographs of the RMS of the adult mouse. (**A**) Closely apposed type A cells (a) form chains flanked by type B cells (b). A cell in mitosis (empty arrow) is present in a chain of type A cells. Two dying cells (d) with picnotic nuclei are present in the periphery of the RMS. (**B**) Pinocytic vesicles (p) adjacent to a zonula adherens–like membrane specialization in the cell membrane of a type A cell (a) with abundant free ribosomes (r) in its cytoplasm. (**C**) Zonula adherens–like membrane specialization (arrow) between two type A cells that shrank during fixation (a). Scale bars: (A), 10 μm; (B), 1 μm; and (C), 2 μm.

a stream of elongated cells oriented in the direction of migration (Fig. 3A). The cell density was much higher in this migratory pathway than in the neighboring parenchyma. In frontal sections, the RMS appeared as circular arrays of densely packed cells (Fig. 4, A, B, and C). Two main cell types were observed in the RMS: (i) Type A cells had a spindle-shaped dark nucleus, with sparse heterochromatin and several nucleoli. These cells had one or two processes oriented in the direction of migration. The cytoplasm of these cells had many free ribosomes (Fig. 3B) and was rich in microtubules. (ii) Type B cells had lighter and larger polymorphic nuclei than type A cells, and they had abundant heterochromatin condensed along the nuclear envelope (Fig. 3A). These cells had several processes oriented in multiple directions. Their cytoplasm was lighter than that of type A cells and rich in intermediate filaments. In addition to type A and type B cells, two other cell types were occasionally found in the RMS: microglia, often associated with dying cells (Fig. 3A), and endothelial cells lining blood vessels.

Type A cells were more abundant than type B cells, in a 3.7:1 ratio (*23*). In sagittal sections, type A cell bodies were closely apposed to each other and formed chains (Fig. 3A). High magnification analysis demonstrated that type A cells displayed membrane specializations that connected neighboring type A cells (Fig. 3, B and C). These membrane specializations had ultrastructural characteristics similar to those described for zonula adherens (*24*). Coated pits were observed between the membranes of adjacent type A cells (Fig. 3B). Some type A cells in the chains were found undergoing mitosis (Fig. 3A).

In sagittal sections, type B cells and their processes flanked the chains of type A cells (Fig. 3A). In frontal sections, type B cells ensheathed the chains of type A cells (Fig. 4, A, B, and C). To investigate the continuity of this arrangement between type A and type B cells in the RMS, we prepared serial frontal sections (*25*). Type A cells were organized into chains that branched and merged along the RMS. These chains contained only the cell bodies and processes of type A cells; no axons or glial processes were observed within these chains. The covering of the chains by type B cells and their processes appeared to be largely continuous in a 26-μm length of RMS that was studied by EM in serial sections (Fig. 4). This arrangement of glial cells covering the chains of migrating neuroblasts was observed at all levels of the RMS studied between the wall of the lateral ventricle up to the core of the olfactory bulb.

Electron microscopy immunocytochemistry showed that type B cells were GFAP positive and that this molecule was specifically localized in bundles of intermediate filaments (*26, 27*). In contrast, type A cells were not stained by GFAP antibodies but instead were immunopositive to PSA–N-CAM (*27*). No specific membrane specializations were found between type A and type B cells.

To confirm that type A cells correspond to the neural precursors that migrate from the SVZ to the olfactory bulb, we gave mice local microinjections of [^{3}H]thymidine in the SVZ (*10*). The ^{3}H-labeled cells that had migrated into the RMS (level indicated by dashed rectangle in Fig. 2A) were identified in semithin sections. Of 40 ^{3}H-labeled cells subsequently identified by EM, all corresponded to type A cells (*28*). We found no ^{3}H-labeled type B cells. Taken together, these results indicate that type A cells are the neural precursors that migrate from the SVZ of the lateral ventricle to the olfactory bulb. These results also suggest that in the adult rodent brain, the glial cells that enwrapped type A cells were not derived from the SVZ of the lateral ventricle.

Vital labeling, immunocytochemical, and ultrastructural analyses indicate that SVZ cells in the brain of adult mice migrate to the olfactory bulb grouped in chains. These chains of migrating neural precursors are flanked by the processes and cell bodies of a type of glial cell that is concentrated along the migratory pathway (Fig. 4). The processes of the glial cells in the RMS enwrap the chains of migrating neuroblasts. These glial cells may play various roles in the migration of SVZ cells in the RMS. They may (i) provide a permissive environment for migration, (ii) provide directional cues for the migration to the olfactory bulb, (iii) restrict the dispersal of neuroblasts outside of the migratory stream, or (iv) isolate the migrating cells from the surrounding parenchyma.

The migration of neural precursors through the brain of the adult mouse is different from that during development (*3, 7*) or in adult birds (*4*). There are no radial glial fibers or axons within the chains that guide the migration of neuroblasts along the RMS. Instead, neuronal precursors in the RMS migrate closely apposed to each other. This migration could occur as individual cells, as groups, or a combination of both. Targeted mutation of the N-CAM gene (*29*), or the enzymatic removal of the polysialic moiety of PSA–N-CAM by endosialidase (*30*), hampers the migration of SVZ cells to the olfactory bulb in newborn mice. PSA–N-CAM may be involved in the grouping of migrating cells into chains or in their interaction with enwrapping glia.

Chain migration allows the movement of large numbers of neuronal precursors through a restricted pathway in the adult brain. This migration occurs at a high speed (30 μm/hour) (*10*) through a complex parenchyma between two regions of the adult brain that are separated by several millimeters. The elucidation of the mechanisms that regulate this form of migration will help explain tangential dispersal of neuro-

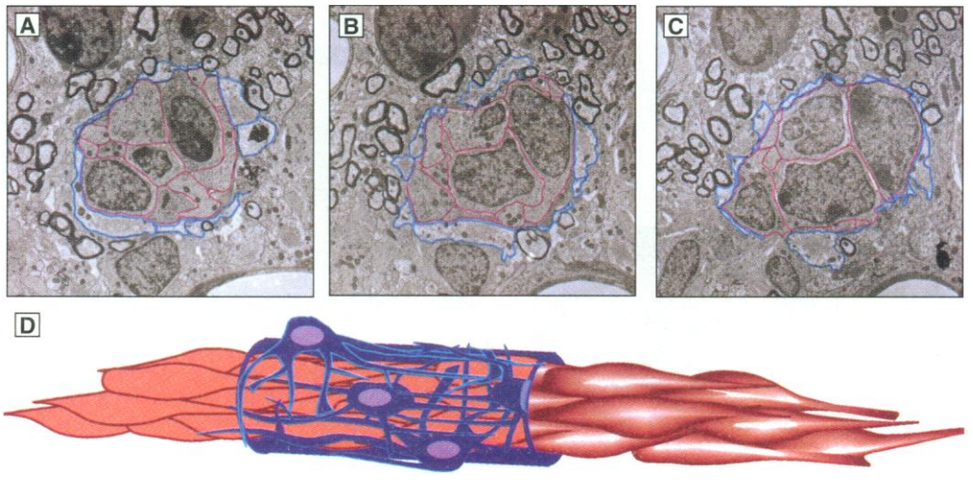

Fig. 4. Electron micrographs of serial cross sections (spaced 1.5 μm) of a chain of neuroblasts in the RMS (**A** to **C**). The contours of type A cells (red) and of processes of type B cells (blue) are highlighted. (**D**) Three-dimensional diagram illustrating the organization of migrating neuroblasts (red spindle-shaped cells) and their relation to flanking glial cells and their processes (blue). Image width for (A), (B), and (C) is ~19 μm.

nal precursors and could be used to steer neuronal precursors to specific locations of the adult brain to replace neurons lost by disease or injury.

REFERENCES AND NOTES

1. Boulder committee, *Anat. Rec.* **166**, 257 (1970); S. K. McConnell, *Brain Res. Rev.* **13**, 1 (1988); M. Jacobson, *Developmental Neurobiology* (Plenum, New York, 1991).
2. K. Herrup and J. Silver, *Curr. Opin. Neurobiol.* **4**, 108 (1994).
3. P. Rakic, *J. Comp. Neurol.* **145**, 61 (1972); *Trends Neurosci.* **4**, 184 (1981); *Experientia* **46**, 882 (1990).
4. A. Alvarez-Buylla and F. Nottebohm, *Nature* **335**, 353 (1988).
5. J. C. Edmondson and M. E. Hatten, *J. Neurosci.* **7**, 1928 (1987).
6. J. Altman, *J. Comp. Neurol.* **137**, 433 (1969).
7. L. Puelles and A. Privat, *Anat. Embryol.* **150**, 187 (1977); S. A. Moody and M. B. Heaton, *J. Comp. Neurol.* **213**, 344 (1983); G. E. Gray, J. C. Clover, J. Majors, J. R. Sanes, *Proc. Natl. Acad. Sci. U.S.A.* **85**, 7356 (1988); F. Bourrat and C. Sotelo, *J. Comp. Neurol.* **294**, 1 (1990); K. Ono and K. Kawamura, *Anat. Embryol.* **182**, 11 (1990); K. Kishi, *J. Comp. Neurol.* **258**, 112 (1987).
8. C. Walsh and C. L. Cepko, *Science* **241**, 1342 (1988); *Experientia* **46**, 940 (1990).
9. M. B. Luskin, *Neuron* **11**, 173 (1993).
10. C. Lois and A. Alvarez-Buylla, *Science* **264**, 1145 (1994).
11. G. Fishell, C. A. Mason, M. E. Hatten, *Nature* **362**, 636 (1993); N. A. O'Rourke, M. E. Dailey, S. J. Smith, S. K. McConnell, *Science* **258**, 299 (1992).
12. J. Altman, *Anat. Rec.* **145**, 573 (1963); S. A. Bayer, J. W. Yackel, P. S. Puri, *Science* **216**, 890 (1982); M. S. Kaplan and J. W. Hinds, *ibid.* **197**, 1092 (1977); F. S. Corotto, J. A. Henegar, J. A. Maruniak, *Neurosci. Lett.* **149**, 111 (1993); P. A. Raymond and S. S. Easter, *J. Neurosci.* **3**, 1077 (1983); S. A. Goldman and F. Nottebohm, *Proc. Natl. Acad. Sci. U.S.A.* **80**, 2390 (1983).
13. J. M. García-Verdugo, I. Farinas, A. Molowny, C. J. Lopez-García, *Morphology* **189**, 189 (1986) .
14. K. Kishi *et al.*, *Arch. Histol. Cytol.* **53**, 219 (1990); S. K. R. Pixley and J. De Vellis, *Dev. Brain Res.* **15**, 201 (1984); T. Voigt, *J. Comp. Neurol.* **289**, 74 (1989); D. E. Schmechel and P. Rakic, *Anat. Embryol.* **156**, 115 (1979); S. M. Culican, N. L. Baumrind, M. Yamamoto, A. L. Pearlman, *J. Neurosci.* **10**, 684 (1990); J. F. Gadisseux, P. Evrard, J. P. Misson, V. S. Caviness Jr., *J. Comp. Neurol.* **322**, 246 (1992).
15. P. Rousselot, C. Lois, A. Alvarez-Buylla, *J. Comp. Neurol.* **351**, 51 (1995).
16. We injected 20 nl of DiI ($DiIC_{18}$, Molecular Probes) into the rostral SVZ (1 mm anterior from bregma, 1 mm lateral from the midline, and 2.3 mm deep from the pial surface) of adult (2- to 4-month-old) male mice (*10*).
17. J.-P. Misson, M. A. Edwards, M. Yamamoto, V. S. Caviness Jr., *Dev. Brain. Res.* **44**, 95 (1988); A. Alvarez-Buylla, D. R. Buskirk, F. Nottebohm, *J. Comp. Neurol.* **264**, 159 (1987).
18. DiI crystals were placed in the olfactory peduncle after removal of the olfactory bulb, or in the SVZ of the rostral part of the lateral ventricle in brains fixed in 3% paraformaldehyde. Brains were incubated for 30 days at 39°C in 3% paraformaldehyde in phosphate-buffered saline. Sections were cut in a Vibratome (50 μm) and mounted with glycerol. In these cases, cells in the RMS were not labeled by DiI, confirming that the DiI-labeled chains observed in the RMS after DiI injection in vivo were due to cell migration.
19. Sections were processed for immunocytochemistry as in (*15*) with mouse monoclonal antibodies to GFAP (Sigma, dilution 1:600) and PSA–N-CAM (dilution 1:150).
20. A. Bignami, L. F. Eng, D. Dahl, C. T. Uyeda, *Brain. Res.* **43**, 429 (1972); A. Bignami and D. Dahl, *J. Comp. Neurol.* **153**, 27 (1974).
21. L. Bonfanti and D. T. Theodosis, *Neuroscience* **62**, 291 (1994).
22. Adult CD-1 male mice (n = 6) were killed by an overdose of pentobarbital and processed for EM as described [C. Lopez-García, A. Molowny, J. M. García-Verdugo, I. Ferrer, *Dev. Brain Res.* **43**, 167 (1988)].
23. Two hundred cells were counted in ×3000 photomicrographs of the intermediate region of the RMS from 11 sections from four animals.
24. M. G. Farquhar and G. E. Palade, *J. Cell Biol.* **17**, 375 (1963); L. A. Stahelin, *Int. Rev. Cytol.* **39**, 191 (1974); D. A. Goodenough and J. P. Revel, *J. Cell Biol.* **45**, 272 (1970).
25. The RMS was sectioned serially in the frontal plane. Semithin (1.5-μm) sections were alternated with seven ultrathin (40- to 50-nm) sections for up to 26 μm. Several chains were photographed in one out of every seven ultrathin sections.
26. Adult CD-1 mice (n = 4) were perfused with 2% paraformaldehyde and 0.2% glutaraldehyde, and their brains were cut into 200-μm sagittal sections. Sections were incubated overnight in 100 mM NH_4Cl, postfixed for 30 min in 0.25% OsO_4, dehydrated and embedded in LRwhite resin (London Resin Company, London), and cut into 60-nm sections. Ultrathin sections were collected onto Formvar-coated nickel grids and processed for immunocytochemistry with antibodies to GFAP (Sigma, dilution 1:2500). Secondary antibodies (Amersham, dilution 1:20) were coupled to 10-nm colloidal gold particles. Sections were then stained with 2% uranyl acetate and examined with a Jeol 100CX electron microscope.
27. C. Lois, J.-M. García-Verdugo, A. Alvarez-Buylla, data not shown.
28. CD-1 male mice (n = 2) received stereotaxic microinjections of [^{3}H]thymidine as described (*10*). Three days after [^{3}H]thymidine administration, the animals were killed and their brains processed for EM as in (*22*). The 2-μm semithin sections were processed for autoradiography and stained with Giemsa, and [^{3}H]thymidine-labeled cells were photographed with a light microscope. Semithin sections were reembedded and cut into 60-nm-thick sections. Ultrathin sections were stained with lead citrate and examined with a Jeol 100CX electron microscope.
29. H. Tomasiewicz *et al.*, *Neuron* **11**, 1163 (1993); H. Cremer *et al.*, *Nature* **367**, 455 (1994).
30. K. Ono, H. Tomasiewicz, T. Magnuson, U. Rutishauser, *Neuron* **13**, 595 (1994).

31. We thank F. Nottebohm, E. Font, and F. Doetsch for critically reading the manuscript, G. Rougon for antibodies to PSA–N-CAM, and E. Sphicas for help with postembedding immunocytochemistry. Supported by NIH grants NS28478 and HD32116 to A.A.B, and DGICYT PB91-0643 (Spain) to J.-M.G.-V. C.L. is a recipient of a La Caixa Foundation graduate program fellowship.

13 September 1995; accepted 21 November 1995

Role of Rho in Chemoattractant-Activated Leukocyte Adhesion Through Integrins

Carlo Laudanna,* James J. Campbell, Eugene C. Butcher

Heterotrimeric guanine nucleotide binding protein (G protein)–linked receptors of the chemoattractant subfamily can trigger adhesion through leukocyte integrins, and in this role they are thought to regulate immune cell-cell interactions and trafficking. In lymphoid cells transfected with formyl peptide or interleukin-8 receptors, agonist stimulation activated nucleotide exchange on the small guanosine triphosphate–binding protein RhoA in seconds. Inactivation of Rho by C3 transferase exoenzyme blocked agonist-induced lymphocyte α4β1 adhesion to vascular cell adhesion molecule–1 and neutrophil β2 integrin adhesion to fibrinogen. These findings suggest that Rho participates in signaling from chemoattractant receptors to trigger rapid adhesion in leukocytes.

Regulated leukocyte adhesion is critical to immunity and inflammation and controls cellular positioning, cell-cell interactions, and immune cell responses. For example, rapid triggering of integrin-mediated adhesion is required for the arrest of blood-borne lymphocytes and neutrophils at sites of leukocyte recruitment from the blood. This extremely rapid and robust adhesion, triggered within a few seconds during leukocyte "rolling" along endothelium, is initiated by pertussis toxin–sensitive $G\alpha_i$-linked receptors of the rhodopsin-related seven transmembrane family (*1*). β2 integrin–mediated arrest of neutrophils, for example, can be triggered through stimulation of the formyl peptide, leukotriene B4, or interleukin-8 (IL-8) chemoattractant receptors in vivo (*1*). The regulation of integrin adhesion through chemoattractant receptors is likely important in cellular locomotion and cell-cell interactions within tissues as well. Intracellular signaling pathways that mediate chemoattractant modulation of calcium flux, neutrophil respiratory burst, and adenyl cyclase activity have been identified (*2*). However, signaling events that control rapid chemoattractant activation of leukocyte integrin adhesion have not been defined.

We used an in vitro model to study the intracellular mechanisms that trigger lymphocyte adhesion through chemoattractant receptors. The mouse L1/2 B lymphoid cell line was transfected with the human formyl peptide receptor (fPR) or with the human IL-8 receptor type A (IL-8RA). Agonist stimulation of these transfectants triggers robust and rapid α4β1-dependent adhesion to purified vascular cell adhesion molecule–1 (VCAM-1) (*3*).

Because chemoattractants including

Laboratory of Immunology and Vascular Biology, Department of Pathology, and Digestive Disease Center, Stanford University, Stanford, CA 94305, USA, and Center for Molecular Biology and Medicine, Veterans Affairs Health Care System, Palo Alto, CA 94304, USA.

*To whom correspondence should be addressed.